Vector Fields for Task-level Distributed Manipulation: Experiments with Organic Micro Actuator Arrays

Karl-Friedrich Böhringer[1,*], *John W. Suh*[2], *Bruce Randall Donald*[1,3], *Gregory T. A. Kovacs*[2]

[1] Robotics & Vision Lab, Dept. of Computer Science, Cornell University, Ithaca, NY 14853

[2] Transducers Lab, Dept. of Electrical Engineering, Stanford University, Stanford, CA 94305

[3] Robotics Lab, Dept. of Computer Science, Stanford University, Stanford, CA 94305

`karl,brd@cs.cornell.edu, jwsuh,kovacs@sensors.stanford.edu`

Abstract

Distributed manipulation experiments were performed using a massively-parallel, microfabricated actuator array. *An organic ciliary array of thin-film polyimide bimorph microactuators exploiting combined thermal and electrostatic control was employed to implement* task-level, sensorless manipulation strategies *for macroscopic objects. The tasks of parts-translation, -rotation, -orientation, and -centering were demonstrated using small integrated circuit (IC) dice. Strategies were programmed in a fine-grained SIMD (single instruction, multiple data) fashion by specifying planar force vector fields. When a part is placed on the array, the programmed vector field induces a force and moment upon it. The part's* equilibrium states *may be predicted and cascaded (using a sequence of fields) to bring the part to a desired final state.*

Vector fields with *and* without potential *were tested in experiments, and the behavior of parts in the fields was compared with the* theory of programmable vector fields. *These fields were implemented by actuating the organic cilia in a cyclic, gait-like fashion. Motion in non-principal (e.g. diagonal) directions was effected by a pairwise coupling of the cilia to implement* virtual cilia. *These experiments suggest that MEMS actuator arrays are useful for parts-orientation, -posing, -transfer, -singulation, and -sorting.*

1 Introduction

The theory of programmable vector fields[1] [2] arguably represents the first systematic attack on massively-parallel distributed manipulation based on geometric and physical reasoning. We report on our experiments in implementing this theory using a microfabricated organic actuator array. These experiments constitute what may be the most convincing evidence to date in support of that theory.

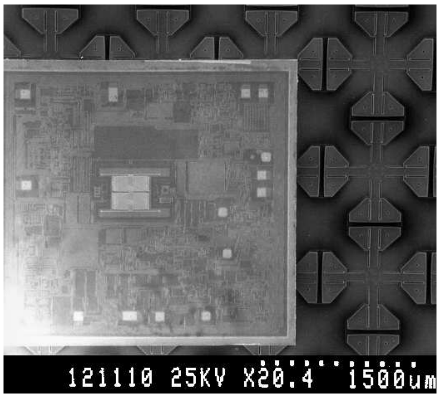

Figure 1: Micro cilia device manipulating an ADXL50 accelerometer chip (courtesy of Dr. R. Payne, Analog Devices, Inc.); its size is 2.7 *mm* squared. The SEM micrograph shows a portion of the cilia chip, which consists of an 8×8 array of motion pixels. The entire device includes four cilia chips that can be controlled independently to generate complex force vector fields.

We performed distributed manipulation experiments using an organic ciliary array of thin-film polyimide bimorph microactuators (Figure 1). The actuators employ independent thermal actuation and electrostatic hold-down. Four orthogonally-oriented actuators are integrated into a unit cell called a "motion pixel" [3]. The motion pixels are replicated to tile a square area, allowing for precise manipulation of small objects placed on top of the array. Our goal was to implement task-level, sensorless manipulation strategies for macroscopic objects. The tasks of parts-translation, -rotation, -orientation, and -centering were demonstrated using small IC dice. Strategies were programmed in a fine-grained SIMD fashion by specifying planar force vector fields. When a part is placed on the array, the programmed vector field induces a force

*Current address: Dept. of Industrial Engineering and Op. Research, University of California at Berkeley, Berkeley, CA 94720.

[1] The theory of programmable vector fields for micro manipulation tasks was introduced in [3].

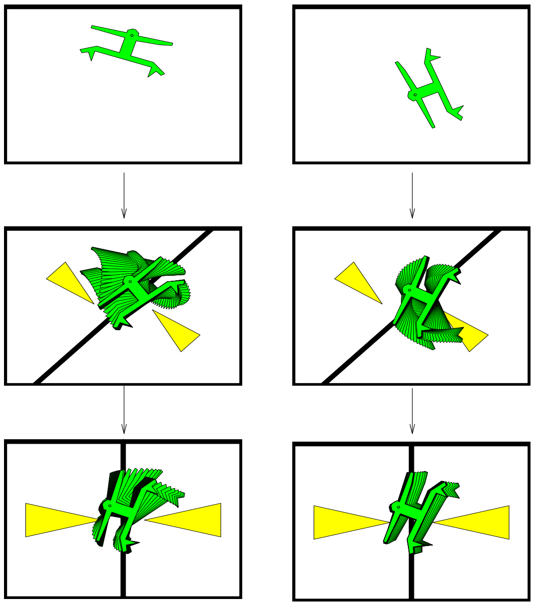

Figure 2: Sensorless parts orienting using force vector fields: The part reaches unique orientation after two subsequent squeezes. There exist such orientating strategies for all polygonal parts. See URL `http://www.cs.cornell.edu/home/karl/MicroManipulation` for an animated simulation. Reproduced from [2].

and moment upon it. Over time, the part may come to rest in a dynamic equilibrium state. By chaining together sequences of vector fields, the equilibrium states of a part in the field may be cascaded to obtain a desired final state—for example, this state may represent a unique orientation or pose of the part (see Figures 2 and 3a-b). The resulting strategies work from any initial configuration (pose) of the part, require no sensing, and enjoy efficient planning algorithms. Our work on programmable vector fields is related to nonprehensile manipulation [4, 12, 5]: in both cases, parts are manipulated without form or force closure.

Even though our fields are typically not smooth, it is possible to define a *potential* for certain fields (as a unique path integral), and to show that when an array ($\mathbb{R}^2$) potential exists, it always lifts to a smooth configuration space ($\mathbb{R}^2 \times \mathbb{S}^1$) potential for the manipulated part [2]. Vector fields with potential have been shown to be theoretically well-suited for manipulation strategies, by classifying a sub-family of potential fields in which every part has stable equilibria [2]. Hence, such fields have been proposed for manipulation tasks in which we desire to cascade equilibria in order to uniquely pose or orient a part [3]. The theory of programmable vector fields permits calculation of stable equilibria for macroscopic parts in potential fields [2] (see Figure 12).[2] In our new experiments, we

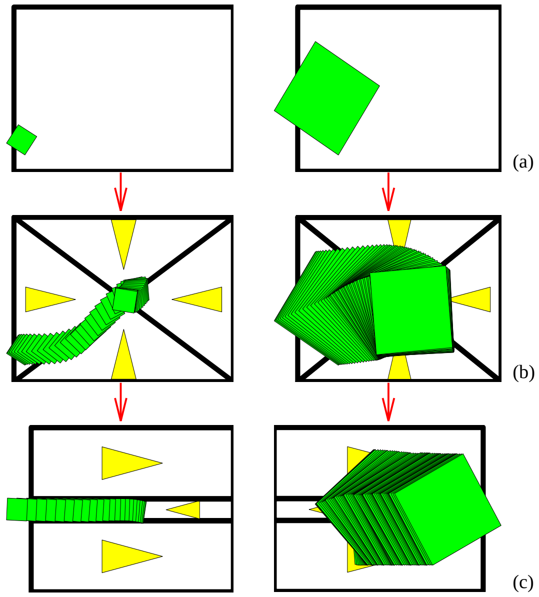

Figure 3: Sensorless sorting using force vector fields: parts of different sizes are first centered and subsequently separated depending on their size. Reproduced from [2].

employed vector fields with potential for parts-orientation and -posing tasks, and the theory was used to predict the equilibrium poses of specific parts (Figure 11). The poses predicted by the equilibrium analysis were observed in our experiments (Figures 10-left).

Perhaps surprisingly, the theory has also predicted the existence of pathological fields which do not induce well-behaved equilibria. In particular, the "lower bounds" of [2] show that there exist perfectly plausible vector fields which induce *no* stable equilibrium in very simple parts. Although these fields are very simple, they result in limit cycles and quite complex behavior. We implemented such fields on the cilia array. Vector fields *without* potential were employed to cast parts into limit cycles, e.g. "infinite" rotation using a skew-symmetric squeeze field. The predicted behavior (Figure 13) for such "unstable" vector fields was also observed (Figure 10-right). This shows that rather complex—but potentially useful—behavior can be generated using very simple fields. We believe our experiments validate the theory and suggest the practicality of such minimalist approaches to distributed manipulation.

The programmable vector fields were implemented by actuating the organic cilia in a cyclic, gait-like fashion. Motion in non-principal (e.g. diagonal) directions was effected by a pairwise coupling of the cilia to implement *virtual cilia* and *virtual gaits,* (analogous to the virtual legs employed by Raibert's hopping and running robots [10]).

These experiments suggest that MEMS actuator arrays are useful for parts-orientation, -posing, -transfer, -singulation, and -sorting. See [2] for more on the promise

[2] While this question has been well-studied for a point mass in a field, the issue is more subtle when lifted to a body with finite area, due to the moment covector. See [2] for details.

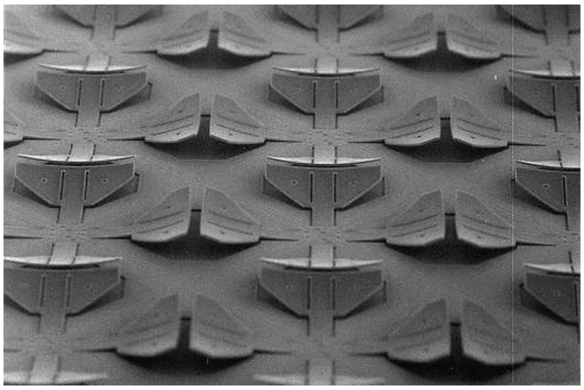

Figure 4: Portion of a polyimide cilia array (SEM micrograph). Four orthogonally-oriented actuators are integrated into a motion pixel, which covers a surface area of approximately $1.1 \times 1.1\, mm^2$.

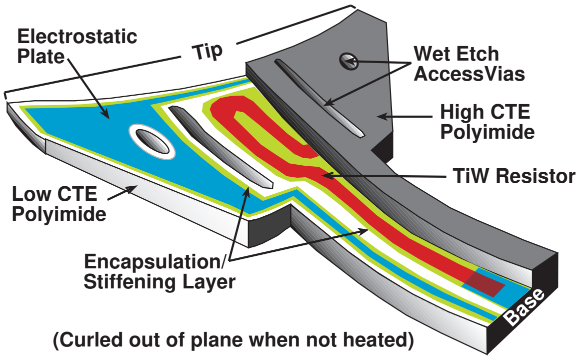

Figure 5: Organic thermal and electrostatic microactuator. Half of the upper polyimide and silicon nitride encapsulation/stiffening layer are shown removed along the cilium's axis of symmetry to show details.

of MEMS arrays for parts feeding. Moreover, the theory of programmable vector fields and virtual gaits gives a method for controlling a very large number of distributed actuators in a principled, geometric, task-level fashion. Whereas many control theories for multiple independent actuators break down as the number of actuators becomes very large, our systems should only become more robust as the actuators become denser and more numerous. This paper represents a step towards testing that theory.

2 Experimental Devices and Setup

Several groups have described efforts to apply MEMS (micro electro mechanical system) actuators to component positioning, inspection, and assembly [9, 1, 7, 3, 8, for example]. The cilia chip [11] employs independent thermal actuation and electrostatic hold-down of an array of 256 thin-film polyimide actuators (Figure 4) grouped together in 64 unit cells. Each cell consists of four orthogonally-oriented actuators called a "motion pixel" [3], because it can generate motion in various directions, spanning the

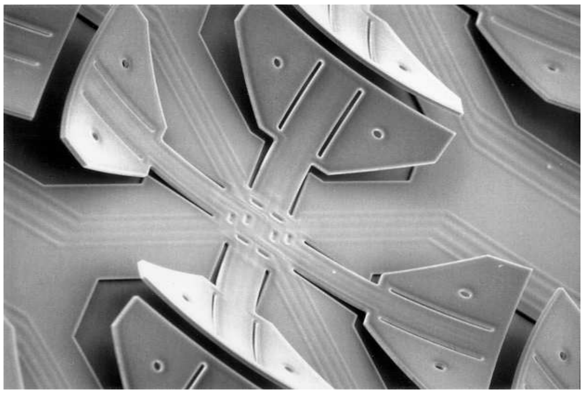

Figure 6: Polyimide cilia motion pixel (SEM micrograph). Four actuators in a common center configuration make up a motion pixel. Each cilium is $430\, \mu m$ long and bends up to $120\, \mu m$ out of the plane.

plane. The motion pixels are replicated to tile a square area, allowing for precise manipulation of small objects placed on top of the array.

Combined Thermobimorph and Electrostatic Actuators. Surface micromachining techniques were used to create the actuators using polyimide as the primary structural material and aluminum as a sacrificial layer. The fabrication process was designed to be compatible with CMOS or BiCMOS circuits which could be prefabricated on a silicon substrate.

Each actuator cilium consists of two layers of polyimide with different thermal expansion coefficients. The cilium also contains a Titanium-Tungsten (Ti:W) resistive heater loop for thermal actuation, Aluminum electrodes for electrostatic (low-power) hold-down, and a silicon nitride encapsulation/stiffening layer (Figure 5). For a detailed description of the fabrication process see [11].

Vertical and horizontal displacements of the cilia tips are a function of the thermal mismatch in the actuator layers. For room temperature, these values can be calculated as $\delta_v \approx 120\, \mu m$ and $\delta_h \approx 20\, \mu m$ [11]. Inspection under the scanning electron microscope (SEM) has verified these calculations.

The lifting capacity of an actuator can be estimated as the force required to deflect the actuator's tip to the substrate. The actuator load capacity has been calculated as $F_l = 76\, \mu m$, which gives a force-per-area ratio of $4 \times 76\, \mu N/(1.1\, mm)^2 \approx 250\, \mu N/mm^2$.

Chip Layout. The cilia array is composed of cells (*motion pixels*, each $1.1 \times 1.1\, mm^2$) which contain four orthogonally-oriented actuators (Figure 6). On the current cilia chip, the motion pixels are arranged in an 8×8 array which occupies approximately $0.77\, cm^2$ of a $1\, cm^2$ die. The four actuators of each pixel are independently activated by four thermal and four electrostatic control lines. Four 8×8 chips were diced and packaged together

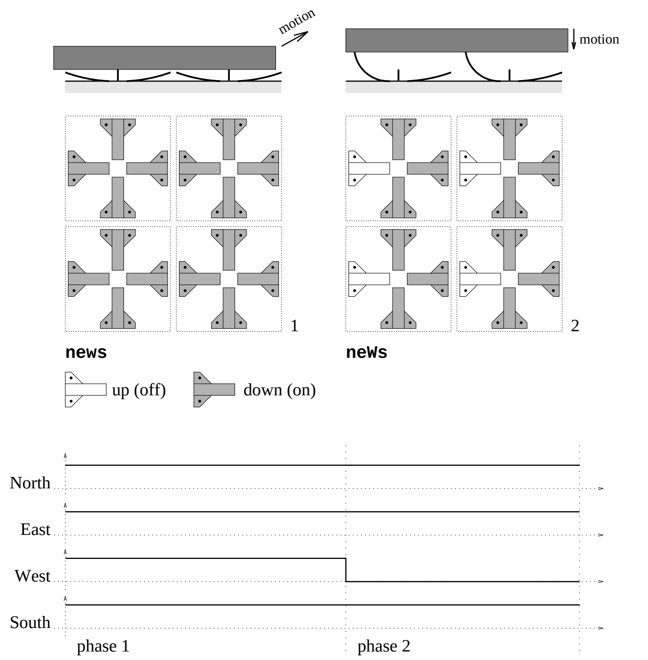

Figure 7: Two-phase gait. The `W` actuator is repeatedly switched on and off, while the other actuators always remain on, resulting in a `news neWs` sequence.

to make a quad-shaped 16×16 cilia array device, with a total of 1024 cilia. The device itself is attached to a hybrid package which is placed on a heat sink and thermo-electric cooler (Peltier effect module). The total input power to the chip can exceed $4\ W$, and without active cooling the package can become very hot. To observe the experiments, a long working distance microscope is connected to a CCD camera, and a video cassette recorder is used to monitor and record both the movements of an individual cilium and the objects conveyed by the array.

Controller. The manipulation results described below were accomplished with the cilia array device interfaced to an IBM 486 personal computer. The PC provides speed control via the drive pulse frequency and directional control interactively via keyboard or mouse, or by actuator programs that can be specified using the MEMSA (MEMS Array) language[3] which we developed at Stanford. The control software including the MEMSA interpreter was written in PASCAL. Thermal and electrostatic control line signals are sent via the PC parallel port to D-type flip-flops which activate power transistors. Currently up to 4 cilia arrays can be controlled simultaneously by using a multiplexer with 2 address bits.

3 Low-level Control: Actuator Gaits

To induce motion on a part that is placed on the array, the cilia are actuated in a cyclic, gait-like fashion.

[3] MEMSA (named after MENSA) is the language for smart manipulation surfaces.

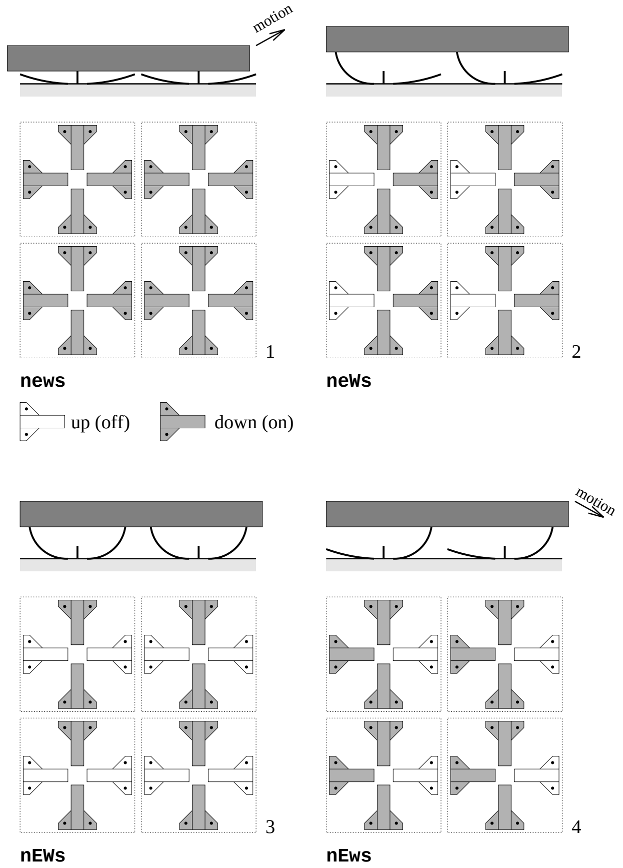

Figure 8: Four-phase gait consisting of the four-pattern sequence `news neWs nEWs nEws`.

In each cycle, the part is moved in a certain direction by the motion of the actuators that are in contact with it. The speed of the moving part depends on the (horizontal) displacement of the actuators per cycle as well as the frequency of cycle repetition. It also depends on the surface properties and weight of the moving part.

Task: Translation of Parts in Principal Directions. The simplest gait is the *two-phase gait*, in which all actuators of the same orientation repeatedly stroke the part while the remaining actuators are held down. Assuming that the orthogonal cilia within a motion pixel are oriented at the principal compass points, let us use capital letters `NEWS` to denote the North, East, West, and South actuators in the up position, and lower-case letters `news` to denote the actuators in the lowered position. Then the two-phase gait to effect motion in the East direction would be `news neWs` (see Figure 7).

The *four-phase gait* consists of four different actuation phases `news neWs nEWs nEws` such that motion is induced during upward as well as downward strokes of the cilia (Figure 8, see also [1]). Note that the forces exerted on the moving part depend on the state of the motion pixel: e.g. in the transition from phase 1 to phase 2 the cil-

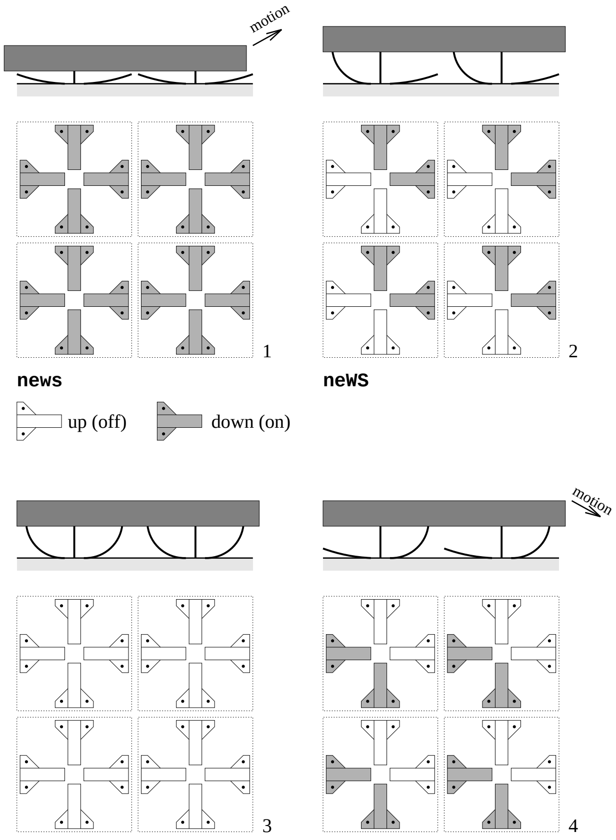

Figure 9: Diagonal (virtual) gait consisting of the four-pattern sequence `news neWS NEWS NEws`. The `N` and `E` cilia, and the `W` and `S` cilia, are coupled to form virtual cilia in North-East and South-West directions.

ium `W` moves up while the opposing cilium `e` remains down. We denote the lateral force exerted on the part in this configuration $f_{\mathtt{W},\mathtt{e}}$. Analogously, during transitions 2–3, 3–4, and 4–1 we observe lateral forces $f_{\mathtt{E},\mathtt{W}}$, $f_{\mathtt{w},\mathtt{E}}$, and $f_{\mathtt{e},\mathtt{w}}$, respectively. $f_{\mathtt{W},\mathtt{e}}$ and $f_{\mathtt{e},\mathtt{w}}$ are in positive x-direction, while $f_{\mathtt{E},\mathtt{W}}$ and $f_{\mathtt{w},\mathtt{E}}$ are negative. Furthermore, from this analysis it follows that $|f_{\mathtt{W},\mathtt{e}}| \gg |f_{\mathtt{e},\mathtt{w}}| \gg |f_{\mathtt{E},\mathtt{W}}| \approx |f_{\mathtt{w},\mathtt{E}}| \approx 0$. Hence we expect a relatively large motion step $\Delta x_{\mathtt{W},\mathtt{e}}$ during transition 1–2, and a smaller step $\Delta x_{\mathtt{e},\mathtt{w}}$ during transition 4–1, while during the other transitions the part remains at its current location. This behavior has been observed in our experiments, where $\Delta x_{\mathtt{W},\mathtt{e}}$ was measured between $3\,\mu m$ and $10\,\mu m$ depending on input power, frequency, surface properties and weight of the part. $\Delta x_{\mathtt{W},\mathtt{e}}$ was usually about twice as large as $\Delta x_{\mathtt{e},\mathtt{w}}$.

Task: Translation of Parts in Arbitrary Directions. Motion in non-principal (e.g. diagonal) directions is effected by a pairwise coupling of two cilia of each pixel, implementing *virtual cilia* analogous to Raibert's concept of virtual legs for hopping and running robots [10]. Hence, several cilia can be coordinated to emulate a virtual cilium, which generates a force corresponding to the vector sum of its components. The diagonal gait to effect motion in the North-East direction would be `news neWS NEWS NEws` where the virtual cilia are `NE` and `WS`. Consequently, we obtain a *virtual gait* that moves the part in a diagonal direction. Note that in a section view through the array looking in the North-West direction, this gait looks virtually identical to the four-phase gait depicted in Figure 8.

Motion in arbitrary directions can be induced by alternating gaits that interleave principal (or virtual) gaits of different directions. For example, a translation at 25° from the x-axis requires motion in the y-direction and x-direction at a ratio of $\tan 25° \approx 1:2$. Our control software determines the exact alternating analogously to the Bresenham line scan algorithm [6], which rasterizes lines at arbitrary angles, resulting in different fields that are interlaced in time.

Experiments and Results. A large number of translation experiments have been performed in which two-phase and four-phase gaits were used to implement principal and virtual gaits. These experiments show that a first-order dynamical system models the device-part interaction well. Therefore, when describing and predicting the motion of parts in force vector fields, we have based our theory on a first-order system (see Section 4).

Silicon chips were moved with a motion resolution of a few μm and speeds up to $200\,\mu m/sec$. Four-phase gaits proved more effective than two-phase gaits, because during the downward motion in the two-phase gait, the part tends to slip backwards. The four-phase gait avoids this effect, because other cilia hold the part in place during the transition 3–4. In the subsequent downward motion in the transition 4–1, the part is also moved forward (Figure 8).

The diagonal gait also has the lowest power consumption (not considering electrostatic hold-down), due to the fact that its duty cycle for cilia hold-down is lowest (50 %), compared to 75 % for the principal four-phase gait, and 87.5 % for the two-phase gait.

As expected, diagonal (virtual) gaits induced the largest and fastest motion because all four cilia of each pixel were activated, whereas in principal gaits only two cilia are actively used, while the others have to be held down continuously (Figure 8).

4 High-level Control: Vector Fields

We believe that vector fields can be used as an *abstraction barrier* between applications requiring array micromanipulation and MEMS devices implementing the requisite mechanical forces. That is, applications such as parts-feeding can be formulated in terms of the vector fields required. This then serves as a specification which the underlying MEMS device technology must deliver. Conversely, the capabilities of MEMS array technologies for actuation can be formulated in terms of the vector fields they can implement. For example, limitations in force

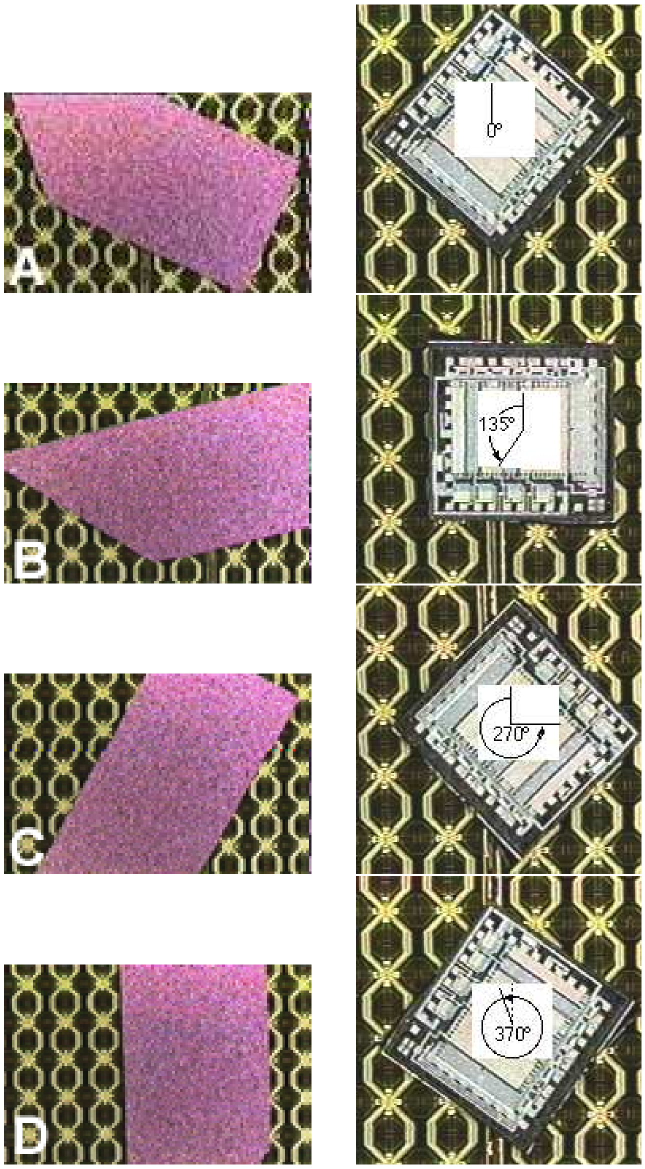

Figure 10: Manipulation of silicon chips in programmable vector fields induced by a micro cilia array (microscope video images).
Left: The chip is aligned with the vertical squeeze line of the field.
Right: Rotating a square-shaped chip counterclockwise in a skewed squeeze field.

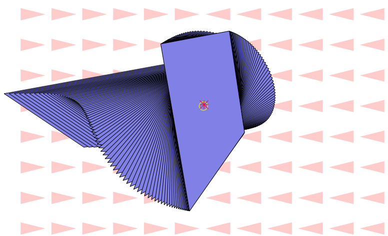

Figure 11: Simulation of alignment task with a squeeze field.

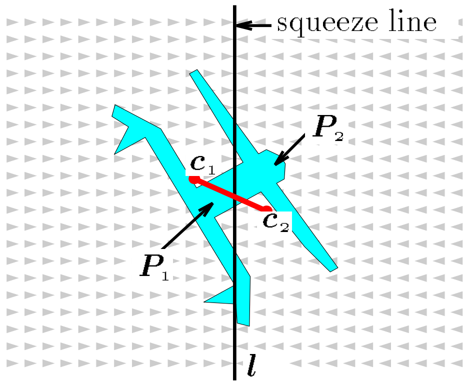

Figure 12: Equilibrium condition: To balance force and moment acting on P in a unit squeeze field, the two areas P_1 and P_2 must be equal (i.e., l must bisect the part), and the line connecting the centers of area c_1 and c_2 must be perpendicular to the squeeze line.

magnitude are naturally expressed in vector field terms, as "small" vector fields. Restrictions in directional selectivity and magnitude control can also be manifested as restrictions on the vector field abstraction (resulting in discretization in orientation or modulus). This means that MEMS designers can potentially ignore certain details of the application process, and instead focus on matching the required vector field specification. Then, once the capabilities of MEMS actuator arrays were published as vector fields and tolerances, an application designer could look in a catalog to choose a device technology based on the field specification it promises to implement. This would free application engineers from needing to know much about process engineering, in the same way that software and algorithm designers often abstract away from details of the hardware. Such an abstraction barrier could permit hierarchical design, and allow application designs with greater independence from the underlying device technology. At the same time, abstraction barriers could allow MEMS array technologies to be designed simultaneously with the (abstract) vector field control. This development pattern could be similar to the concurrent design of VLSI processors with their compilers, as is common in computer architecture.

4.1 Squeeze Fields

In [3], Böhringer and Donald proposed a family of control strategies called *squeeze fields* and a planning algorithm for parts-orientation (see Figures 2 and 12).

Definition 1 [2] *Given a straight line l, a* squeeze field *f is a two-dimensional force vector field in which, at each point, a unit force points perpendicularly towards l (on l the force is zero).*

We refer to the line l as the *squeeze line*, because l lies in the center of the squeeze field.

Assuming quasi-static motion, an object will translate and rotate to an equilibrium configuration, as characterized in Figure 12. This assumes a uniform force distribution over the surface of P, which is a reasonable assumption for a flat part that is in contact with a large number of elastic actuators.

Definition 2 *A part P is in* translational equilibrium *if the forces acting on P are balanced. P is in* orientational equilibrium *if the moments acting on P are balanced.* Total equilibrium *is simultaneous translational and orientational equilibrium.*

Claim 3 [2] *Every squeeze field f (see Definition 1) has potential, of the form $U(\mathbf{z}) = \int_\alpha f \cdot ds$, where α is an arbitrary path to $\mathbf{z}$ from a fixed reference point. If $d_{\mathbf{z}}$ denotes the perpendicular distance of $\mathbf{z}$ from the squeeze line, then $U(d_{\mathbf{z}}) = |d_{\mathbf{z}}|$.*

Claim 4 [2] *Let P be a connected polygonal part with finite contact area and n vertices. Then in any squeeze field, P has $O(kn^2)$ orientation equilibria, where k is the maximum number of edges that a bisector of P can cross. If P is convex, then the number of equilibria is $O(n)$.*

Equilibria can be calculated numerically or, for polygonal parts, exactly: see Figure 12 and [2] for details.

Claim 5 [2] *Let P be a polygon whose interior is connected. There exists a sensorless alignment strategy consisting of a sequence of squeeze patterns that uniquely orients P up to symmetries.*

Task: Orienting and Aligning Parts

If a part is placed in a squeeze field, it will translate and rotate until a stable equilibrium is reached (Claim 4). Parts may exhibit several equilibria, hence after one squeeze the part orientation may be ambiguous. This ambiguity can be removed with the strategies of Claim 5: by executing a sequence of squeezes at particular angles, the part is uniquely oriented (see Figure 2, for details see [2]).

Experiments and Results. The long, thin part depicted in Figures 10-left and 11 exhibits a unique stable equilibrium (modulo 180° field symmetry). When placed in a squeeze field, its longitudinal axis aligns with the squeeze line. This dynamical process is predicted by simulation in Figure 11, and verified in experiment (see Figure 10-left). This part alignment experiment has also been performed with similar results for several other small pieces of glass and silicon of a few mm length and several mg of mass.

4.2 Skewed Squeeze Fields

Definition 6 [2] *A* skewed field f_S *is a vector field given by $f_S(x, y) = -\mathrm{sign}(x)(1, \epsilon)$, where $0 \neq \epsilon \in \mathbb{R}$.*

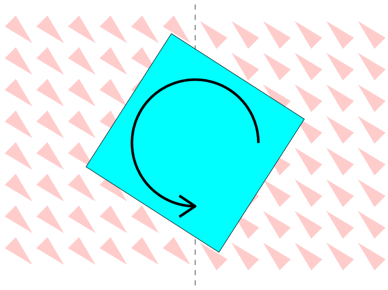

Figure 13: Unstable square-shaped part in a skewed squeeze field ($\epsilon = -1$). The square with center on the squeeze line will rotate indefinitely. Moreover, it has *no* stable equilibrium in this field.

Claim 7 [2] *No skewed squeeze field has a potential.*

Claim 8 [2] *A skewed field induces* no *stable equilibrium on a disk-shaped part (for all $\epsilon \neq 0$).*

Claim 9 *A diagonally skewed field ($\epsilon = \pm 1$) induces* no *stable equilibrium on a square-shaped part.*

Task: Rotating Parts

According to Claims 8 and 9, certain parts will rotate indefinitely in skewed squeeze fields (Figure 13). Note that even though our cilia device has more degrees of freedom, two areas of constant force are sufficient to implement a skewed field, resulting in a very simple task-level rotation strategy. In particular, the rotation algorithm resulting from the application of skew-symmetric squeeze fields is considerably simpler than rotation algorithms proposed in the MEMS literature (for example, the vortices suggested by Fujita [7] or by Liu and Will [8]). Vortices require at least four areas of the array to be pushing in different directions. That is, vortices can be implemented using four triangular or rectangular regions, upon each of which the vector field is constant. Skewed fields perform the same task with only two regions of constant force.

Experiments and Results. Figure 10-right shows video frames of a 3×3 mm^2 IC chip rotating on the squeeze line of a skewed field. During the experiments of approximately 10 min, several full rotations of the part were performed.

4.3 Radial Fields

Definition 10 *A radial field f is a two-dimensional force vector field such that $f(\mathbf{z}) = -\mathbf{z}/|\mathbf{z}|$ if $\mathbf{z} \neq 0$, and $f(\mathbf{0}) = \mathbf{0}$.*

Claim 11 [2] *A radial field has a potential, $U(\mathbf{z}) = |\mathbf{z}|$.*

Claim 12 [2] *Given a polygonal part P in a radial field f, there exists a unique* pivot point *v of P such that P is in equilibrium if and only if v coincides with the center of the radial field.*

Task: Centering Parts

Radial fields can be used to center a part. With the current four-quadrant cilia device, we have implemented an approximation of an ideal radial field similar to the field in Figure 3-b. Note that this approximate radial field has a potential.

Experiments and Results. Small silicon and glass parts were centered using our cilia device. In this experiment, high positioning accuracy (in the μm range) was hard to achieve, because the center of the radial field coincides with the the location of the dice edges. Manual packaging of the four cilia chips leaves small gaps and non-planarities at these junctions. The next generation cilia device will overcome this problem, because it will allow us to implement the radial field with a single chip. Furthermore, because of its full pixel-wise programmability, the new chip will allow us to closely approximate ideal radial fields.

5 Conclusions

Small parts (sizes in the *mm* range) were successfully manipulated using an organic MEMS cilia array. The experiments demonstrated parts-translation, -rotation, -orientation, and -centering of IC dice, and other small pieces of silicon and glass, as predicted by the *theory of programmable vector fields*. With this theory, force vector fields can be cascaded into *multi-step strategies*. It has been shown that these open-loop strategies can sort as well as uniquely position and orient a parts without sensor feedback.

Based on our experiments, we are currently fabricating a new, improved array. Benefits of this fully programmable cilia array will include among others the implementation of sequences of squeeze fields, nearly-ideal radial fields, and sensorless sorting strategies. The new design will overcome current problems due to manual packaging.

Acknowledgements

The authors would like to thank Steve Glander, Robert Darling, Christopher Storment, and the members of the Stanford Transducers Lab; Noel MacDonald and the members of his research team; and Lydia Kavraki.

Support was provided in part by the NSF under grants no. IRI-8802390, IRI-9000532, IRI-9201699, IRI-9530785, and by a Presidential Young Investigator award to Bruce Donald, in part by NSF/ARPA Special Grant for Experimental Research no. IRI-9403903, and in part by the AFOSR, the Mathematical Sciences Institute, Intel Corporation, and AT&T Bell laboratories. This research obtained initial ARPA sponsorship under grant no. N00014-92-J-1940.

References

[1] M. Ataka, A. Omodaka, and H. Fujita. A biomimetic micro motion system. In *Transducers — Digest Int. Conf. on Solid-State Sensors and Actuators*, pages 38–41, Pacifico, Yokohama, Japan, June 1993.

[2] K.-F. Böhringer, B. R. Donald, and N. C. MacDonald. Upper and lower bounds for programmable vector fields with applications to MEMS and vibratory plate parts feeders. In *International Workshop on Algorithmic Foundations of Robotics (WAFR)*, Toulouse, France, July 1996. `http://www.cs.cornell.edu/home/karl/MicroManipulation`.

[3] K.-F. Böhringer, B. R. Donald, R. Mihailovich, and N. C. MacDonald. A theory of manipulation and control for microfabricated actuator arrays. In *Proc. IEEE Workshop on Micro Electro Mechanical Systems (MEMS)*, pages 102–107, Oiso, Japan, Jan. 1994. `http://www.cs.cornell.edu/home/karl/MicroActuators`.

[4] B. R. Donald, J. Jennings, and D. Rus. Information invariants for distributed manipulation. In K. Goldberg, D. Halperin, J.-C. Latombe, and R. Wilson, editors, *International Workshop on Algorithmic Foundations of Robotics (WAFR)*, pages 431–459, Wellesley, MA, 1995. K. Peters.

[5] M. A. Erdmann. An exploration of nonprehensile two-palm manipulation: Planning and execution. Technical report, Carnegie Mellon University, Pittsburgh, PA, 1996.

[6] J. D. Foley, A. Van Dam, Feiner, and Hughes. *Computer Graphics: Principles and Practice.* Addison Wesley, 2 edition, 1996.

[7] H. Fujita. Group work of microactuators. In *International Advanced Robot Program Workshop on Micromachine Technologies and Systems*, pages 24–31, Tokyo, Japan, Oct. 1993.

[8] W. Liu and P. Will. Parts manipulation on an intelligent motion surface. In *IROS*, Pittsburgh, PA, 1995.

[9] K. S. J. Pister, R. Fearing, and R. Howe. A planar air levitated electrostatic actuator system. In *Proc. IEEE Workshop on Micro Electro Mechanical Systems (MEMS)*, pages 67–71, Napa Valley, California, Feb. 1990.

[10] M. H. Raibert, J. K. Hodgins, R. R. Playter, and R. P. Ringrose. Animation of legged maneuvers: jumps, somersaults, and gait transitions. *Journal of the Robotics Society of Japan*, 11(3):333–341, 1993.

[11] J. W. Suh, S. F. Glander, R. B. Darling, C. W. Storment, and G. T. A. Kovacs. Combined organic thermal and electrostatic omnidirectional ciliary microactuator array for object positioning and inspection. In *Proc. Solid State Sensor and Actuator Workshop*, Hilton Head, NC, June 1996.

[12] N. B. Zumel and M. A. Erdmann. Nonprehensile two palm manipulation with non-equilibrium transitions between stable states. In *Proc. IEEE Int. Conf. on Robotics and Automation (ICRA)*, Minneapolis, MN, Apr. 1996.